Water at Hydrophobic Surfaces: Weak Hydrogen Bonding and Strong Orientation Effects

L. F. Scatena *et al.*

This copy is for your personal, non-commercial use only.

When D is reduced, the surface-to-volume ratio grows roughly as $1/D$. Consequently, volume contributions to the free energy (e.g., intermolecular potential and entropy), which are the basis of the known phase diagram (*26–28*), are progressively balanced by interfacial contributions (*29*). Under confinement, cyclohexane is known to exhibit a depression of phase-transition temperatures (*2, 30–32*) and a reduction of normalized enthalpies (*32*), as well as lower critical points (*31, 33, 34*). Macroscopic thermodynamics are inadequate to describe the properties of small volumes, being defined for infinite ensembles of particles. In small volumes, however, thermal fluctuations become increasingly important, and a time-averaged definition of thermodynamic functions is more useful (*35*).

To change the density of bulk cyclohexane from the solid state to the gas phase, an energy, W, of at least 36 kJ/mol (heat of melting plus heat of vaporization) is required. This energy is more than 10 times the kinetic energy, kT, available for thermal fluctuations. Homogeneous density fluctuations of the observed magnitude can only be thermal in nature if a reduction of W, by at least a factor of 10, is effective in this 2-nm-wide mica pore. This simple estimate is in excellent agreement with the sixfold reduction in transition enthalpies for cyclohexane in 4-nm porous silica, measured by means of DSC (*32*).

Molecules within 2 to 3 nm of the surface are thought to form a layer of thermally fluctuating optical and mechanical properties, as a consequence of the surface-induced decoupling of energy and density changes. This may explain many observations in confined cyclohexane, such as the time-averaged density reduction (Fig. 2B), density fluctuations (Fig. 2B), critical scattering (*36*), high surface mobility (*4, 37*), anomalously fast self diffusion (*3, 33*), modified molecular dynamics (*33, 34*) and macroscopic mechanical properties, such as apparent solidification (*17, 38*), and excluded-volume effects leading to quasi-periodic film-thickness transitions (Fig. 2A). Additional insights into the fascinating properties of confined fluids are expected from a planned laterally resolved real-time measurement of D and n in the eSFA.

References and Notes
1. H. K. Christenson, R. G. Horn, J. N. Israelachvili, *J. Colloid Interface Sci.* **88**, 79 (1982).
2. C. Faivre, D. Bellet, G. Dolino, *Eur. J. Phys. B* **7**, 19 (1999).
3. J. C. Dore, M. Dunn, T. Hasebe, J. H. Strange, *Colloids Surf.* **36**, 199 (1989).
4. D. W. Aksnes, L. Gjerdåker, *J. Mol. Struct.* **475**, 27 (1999).
5. M. Heuberger, *Rev. Sci. Instrum.* **72**, 1700 (2001).
6. P. Kékicheff, O. Spalla, *Langmuir* **10**, 1584 (1994).
7. M. M. Kohonen, H. K. Christenson, *Langmuir* **16**, 7285 (2000).
8. J. N. Israelachvili, *J. Colloid Interface Sci.* **44**, 259 (1973).
9. B. Gauthier-Manuel, J.-P. Gallinet, *J. Colloid Interface Sci.* **175**, 476 (1995).
10. H. K. Christenson, *Colloids Surf. A* **123-124**, 355 (1996).
11. J. Janik, R. Tadmor, J. Klein, *Langmuir* **13**, 4466 (1997).
12. V. Kitaev, E. Kumacheva, *J. Phys. Chem. B* **104**, 8822 (2000).
13. H. Hertz, *J. Reine Angew. Math.* **92**, 156 (1881).
14. K. L. Johnson, K. Kendall, A. D. Roberts, *Proc. R. Soc. London A* **324**, 301 (1971).
15. R. G. Horn, J. N. Israelachvili, F. Pribac, *J. Colloid Interface Sci.* **115**, 480 (1987).
16. M. L. Gee, P. M. McGuiggan, J. N. Israelachvili, A. M. Homola, *J. Chem. Phys.* **93**, 1895 (1990).
17. E. Kumacheva, J. Klein, *J. Chem. Phys.* **108**, 7010 (1998).
18. H. Farman, F. M. Coveney, J. C. Dore, *Physica B* **180-181**, 857 (1992).
19. J. Israelachvili, *Intermolecular & Surface Forces* (Academic Press, London, ed. 2, 1991).
20. Supplementary data is available at www.sciencemag. org/cgi/content/full/292/5518/905/DC1
21. H. K. Christenson, *J. Chem. Phys.* **78**, 6906 (1983).
22. O. Hassel, A. M. Sommerfeldt, *Z. Phys. Chem. B* **40**, 391 (1938).
23. J. H. Gladstone, J. Dale, *Philosophical Transactions* **153**, 317 (1863).
24. G. Godbout, Y. Sicotte, *J. Chim. Phys.* **65**, 1944 (1968).
25. C. Wohlfarth, B. Wohlfarth, in *Landolt-Börnstein, Numerical Data and Functional Relationships in Science and Technology*, M. D. Lechner, Ed., Group III, *Condensed Matter* (Springer, Weinheim, Germany, ed. 5, 1987), vol. 38.
26. K. D. Wisotzki, A. Würflinger, *J. Phys. Chem. Solids* **43**, 13 (1982).
27. L. Schulte, A. Würflinger, *J. Chem. Thermodyn.* **19**, 363 (1987).
28. J. Mayer *et al.*, *Phys. Status Solidi B* **166**, 381 (1991).
29. R. Evans, M. B. Marconi, *J. Chem. Phys.* **86**, 7138 (1987).
30. S. M. Ross, J. H. Strange, *Mol. Cryst. Liq. Cryst. Sci. Technol.* **33**, 321 (1976).
31. C. L. Jackson, G. B. McKenna, *J. Chem. Phys.* **93**, 9002 (1990).
32. R. Mu, V. M. Malhotra, *Phys. Rev. B* **44**, 4296 (1991).
33. S. Stapf, R. Kimmich, T. Zavada, *Appl. Magn. Reson.* **12**, 199 (1997).
34. H. F. Booth, J. H. Strange, *Mol. Phys.* **93**, 263 (1998).
35. T. L. Hill, *Thermodynamics of Small Systems* (Dover, New York, 1994).
36. J. B. W. Webber, J. C. Dore, H. Fischer, L. Vuillard, *Chem. Phys. Lett.* **253**, 367 (1996).
37. H. F. Booth, J. H. Strange, *Magn. Reson. Imaging* **16**, 501 (1998).
38. J. Klein, E. Kumacheva, *Science* **269**, 816 (1995).
39. J. N. Israelachvili, G. E. Adams, *J. Chem. Soc. Faraday Trans. I* **74**, 975 (1978).
40. J. N. Israelachvili, P. M. McGuiggan, *J. Mater. Res.* **5**, 2223 (1990).
41. We acknowledge the excellent technical support provided by J. Vanicek and M. Elsener and stimulating scientific discussions with Y. Y. Podladchikov, A. J. Gellman, and H. Ch. Öttinger. We are also most grateful for useful insights from an anonymous reviewer. Financed by the Swiss National Science Foundation (M.Z.) and the Holderbank Stiftung (M.H.). More information about the extended surface forces apparatus and these experiments are available at www.surface.mat.ethz.ch/users/manfred/eSFA.

22 December 2000; accepted 21 March 2001

Water at Hydrophobic Surfaces: Weak Hydrogen Bonding and Strong Orientation Effects

L. F. Scatena, M. G. Brown, G. L. Richmond*

Vibrational studies that selectively probe molecular structure at CCl_4/H_2O and hydrocarbon/H_2O interfaces show that the hydrogen bonding between adjacent water molecules at these interfaces is weak, in contrast to generally accepted models of water next to fluid hydrophobic surfaces that suggest strong hydrogen bonding. However, interactions between these water molecules and the organic phase result in substantial orientation of these weakly hydrogen-bonded water molecules in the interfacial region. The results have important implications for understanding water adjacent to hydrophobic surfaces and the penetration of water into hydrophobic phases.

Protein folding, membrane formation, micellar assembly, and wetting are a few of the many processes in which the interaction of water with hydrophobic fluid surfaces plays an important role. A driving force behind these processes is an uncommonly large entropy loss, which is usually explained as an enhanced structuring of water in the immediate vicinity of apolar molecules, biological macromolecules, and hydrophobic surfaces. Experimental measurements that provide a molecular-level view of interfacial water structure and hydrogen bonding at these interfaces have proven to be problematic because of the difficulty in selectively examining interfacial water molecules. Hence, most of our understanding of the molecular structure of water at hydrophobic surfaces comes from theory (*1–7*). Here we report surface-specific vibrational spectroscopy experiments on the CCl_4/H_2O and hexane/H_2O interfaces, which provide detailed information on the structure and orientation of water influenced

Department of Chemistry, University of Oregon, Eugene OR 97403, USA.

*To whom correspondence should be addressed. E-mail: richmond@oregon.uoregon.edu

by interaction with a hydrophobic liquid. These vibrational sum frequency studies show that a large portion of interfacial water molecules have remarkably weak or negligible hydrogen bonding interactions with other interfacial water molecules, in contrast to the enhanced water structure commonly invoked by the standard picture of hydrophobic hydration. These weakly interacting interfacial water molecules nevertheless are oriented by interactions with the organic phase, and some can change orientation with variation of the aqueous-phase pH.

We used total internal reflection (TIR) vibrational sum frequency spectroscopy (VSFS) (8–10) in these studies as a molecular probe of the hydrogen bonding and orientation of interfacial water molecules at organic/water interfaces and compared the results with similar measurements at the vapor/water interface. The SF vibrational spectrum results from a summation of the optical frequencies of two incident laser beams: a fixed visible beam and a tunable infrared (IR) beam that pass through the organic media and illuminate the interface. This second-order optical process is forbidden in the centrosymmetric bulk liquid phases but will occur at the interface of the two liquids where inversion symmetry is broken.

The anomolously high surface tension at a vapor/water interface is generally recognized to be the result of strong hydrogen bonding between surface water molecules (11). At organic/water interfaces, the interfacial tension is known to decrease with the polarity of the organic phase until the phases are miscible. Figure 1 compares the vibrational spectrum of the OH stretching modes of water at these interfaces for the CCl_4/H_2O (Fig. 1A), hexane/H_2O (Fig. 1B), and vapor/H_2O (Fig. 1C) systems (12). The frequencies of these modes are known to be highly sensitive to intermolecular hydrogen bonding between water molecules. As the hydrogen bonding interactions between water molecules decrease, a strengthening of the OH oscillator results in a blue shift in energy and a sharpening of spectral peaks (13). The most obvious difference between the spectra of Fig. 1 is that the organic/water interfaces are dominated by spectral intensity at higher frequencies (weaker H_2O-H_2O interactions) relative to the vapor/water interface (Fig. 1C). In the case of the vapor/water interface, the strong spectral intensity at lower energies (3100 to 3400 cm^{-1}) is characteristic of tetrahedrally coordinated water molecules participating in strong hydrogen bonding interactions with adjacent surface water molecules. The majority of water molecules at this interface are involved in extensive hydrogen bonding (14). In contrast, the CCl_4/H_2O (Fig. 1A) and hexane/H_2O (Fig. 1B) interfaces are dominated by intensity at higher energies (3400 to 3700

cm^{-1}) characteristic of weakly and non–hydrogen-bonded water molecules (15–17). The VSF spectrum of 1-hexene/water (not shown) is similar (18).

The VSF spectra shown in Fig. 1 represent all water molecules in the interfacial region that are perturbed by asymmetric forces that occur between the two dissimilar phases. The spectra thus demonstrate that the hydrogen-bonding interactions between water molecules at the organic/water interface are greatly reduced relative to those at the vapor/water interface. This weakening of hydrogen bond interaction arises from a reduction in the coordination number of interfacial water molecules and/or a weakening in the strength of individual hydrogen bonds between interfacial water molecules as they interact with the organic phase.

Further experiments have allowed the identification and characterization of the different interfacial water species giving rise to the spectrum in Fig. 1A. All spectra display a sharp peak at higher energies, at ~3700 cm^{-1} and 3669 ± 1 cm^{-1} for the vapor/water (9, 14) and CCl_4/H_2O interfaces, respectively, with a weaker but measurable peak at 3669 ± 4 cm^{-1} for the hexane/water interface. This peak corresponds to the "dangling bond" or "free OH bond" of water molecules that straddle the interface, this bond being the one that protrudes into the organic or vapor phase. This OH stretch mode is energetically uncoupled from its adjoining OH bond that is directed into the aqueous phase where it hydrogen bonds to other water molecules. The red shift of the free OH bond energy for all liquid/liquid interfaces studied here relative

to the free OH bond of the vapor/water interface (Fig. 1C) indicates an attractive interaction between this free OH bond and the interfacial organic molecules. (19) To confirm this, IR absorption measurements of HOD in CCl_4 were conducted (Fig. 2A) (20). Isotope experiments such as these are important because the vibrational spectrum of HOD is much simpler than that of H_2O because of a reduction in intra- and intermolecular coupling, which broadens the spectral features in the case of H_2O (21–25). Under the conditions employed, where only monomeric HOD and D_2O are present in CCl_4, the Fourier transform infrared (FTIR) spectrum of HOD in CCl_4 displays a single peak at 3663 cm^{-1} (Fig. 2A). This peak corresponds to the uncoupled OH stretch mode of HOD and is similar in energy to the uncoupled free OH bond mode of Fig. 1A.

To obtain the OH spectrum of the adjoining OH bond of the molecules that straddle the interface (the bond that is directed into the aqueous phase), VSF measurements of HOD at the CCl_4/H_2O interface were made (Fig. 2B). The VSF spectrum of HOD shows the free OH mode peak at 3667 cm^{-1} (Fig. 2B) and a broader peak at 3450 cm^{-1}, which we attribute to the uncoupled OH stretch mode of interfacial HOD molecules that have an OH bond protruding into the aqueous phase. The energy and breadth of this peak relative to the free OH bond mode confirm that it is hydrogen bonding with other water molecules. Hence, the spectrum in Fig. 2B represents the effective VSF spectrum of the portion of interfacial H_2O molecules in Fig. 1A composed of a free and
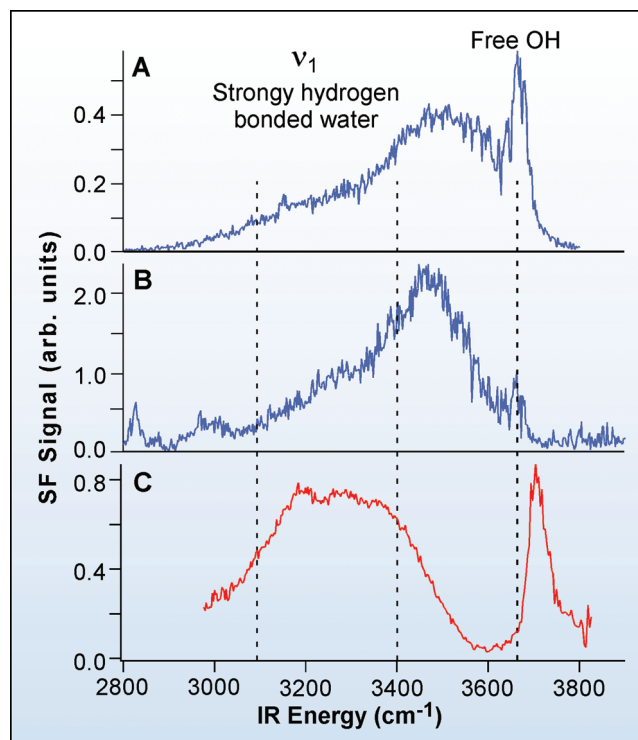
Fig. 1. VSF spectra of the CCl_4/water (**A**), hexane/water (**B**), and vapor/water interfaces (**C**), indicating the differences in hydrogen bonding at the various interfaces. Intensity variations in the 2800 to 3000 cm^{-1} region for hexane/water are due to absorption of the incident IR beam by CH stretching modes in the bulk hexane phase, making quantitative comparison in this region with the other two spectra not appropriate.

bonded OH bond, because these H_2O molecules (molecules that straddle the interface) have similar vibrational decoupling to that of HOD. This leads us to conclude that a substantial portion of the intensity in the 3450 cm^{-1} region of the spectrum in Fig. 1A is due to the bonded OH mode of these water molecules that straddle the interface. Polarization experiments confirm that both of these adjoining OH bonds have a perpendicular component and do not lie exactly parallel to the interfacial plane.

The remaining portion of the H_2O spectrum of Fig. 1A that has not yet been explained is in the 3600 cm^{-1} region at slightly lower energy than the free OH bond mode. Because the weakest interacting water molecules that could be present at the interface would be water monomers surrounded by CCl_4, we measured the IR spectrum of a solution of water monomers in CCl_4 (Fig. 3A). The OH stretch of these monomers shows two characteristic peaks: the symmetric OH stretch (SS, or ν_1) at 3616 cm^{-1} and the asymmetric OH stretch (AS, or ν_3) at 3708 cm^{-1} that bracket the free OH bond stretch mode in the CCl_4/H_2O VSF spectrum shown for comparison in Fig. 3B. The energy of the SS mode corresponds well with the VSF intensity in the 3600 cm^{-1} region of CCl_4/H_2O. Hence, the spectral intensity in this region must correspond to interfacial water molecules that have weak H_2O-H_2O or CCl_4-H_2O bonding interactions comparable to the CCl_4-H_2O interactions in bulk CCl_4; that is, monomeric interfacial water molecules whose sole interaction is with CCl_4 (monomers) and hydrogen bond acceptor interfacial water molecules that hydrogen bond to other water molecules through the lone electron pairs on the oxygen atom (HB acceptor).

Because VSFS is a coherent process, neighboring resonant vibrational modes can interfere in a constructive or destructive manner, depending on the inherent phase (26) and orientation of the molecular vibration. (27–29) The intensity in the 3600 cm^{-1} region of CCl_4/H_2O is consistent with constructive interference between the free OH bond mode and the SS mode of interfacial H_2O monomers/HB acceptors. Given that the free OH bond mode has a substantial perpendicular component relative to the interface, constructive interference between this mode and the SS of the monomer/HB acceptor molecules can only occur if their dipole is in the same orientation; that is, oriented with their hydrogen atoms pointed into the CCl_4 phase (27). Because under I_{SSP} polarization, the SS and AS of monomeric/HB acceptor are 180° out of phase (27), the SF response from the AS mode of such oriented water monomers/HB acceptors results in destructive interference near 3700 cm^{-1} with the free OH bond mode. This would be manifested by a relatively

sharp drop in intensity on the high-energy side of the free OH bond mode, as is observed in Fig. 1A.

Further evidence confirming the orientation and presence of these oriented monomer/HB acceptor water molecules at the interface comes from experiments in which the aqueous-phase pH varied. As the pH is altered (Fig. 3, C and D), distinct changes are observed in the monomeric AS and SS regions. At low pH and up until neutral pH, very little change is observed in these regions (compare Fig. 3, B and D). At higher pH (Fig. 3C), a distinct decrease in intensity in the SS region and an increase in the AS region is observed, indicating a change in the average orientation

of these monomeric/HB acceptor molecules of ~180°. This flip in orientation of the molecular dipole and the corresponding ~180° phase change result in the SS intensity becoming out of phase and the AS becoming in phase with the free OH bond as observed. No change was observed in ionic strength studies using NaCl as a solute. We attribute the flip in orientation observed for these interfacial water molecules to a change in interfacial potential caused by the change in interfacial OH$^-$ concentration.

A best fit to the data based on spectral peak positions and widths of the contributing OH stretching modes of water derived from the isotope and IR spectroscopic measure-
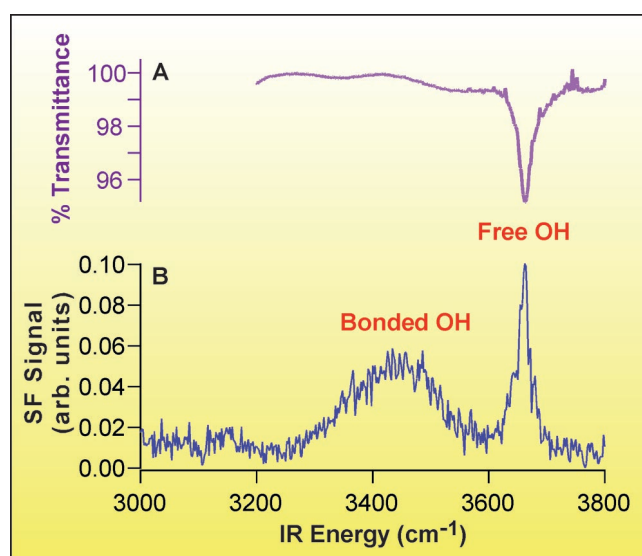

Fig. 2. Isotopic exchange studies in bulk CCl_4 and at the CCl_4/water interface. (**A**) FTIR spectrum of HOD in bulk CCl_4. (**B**) VSF spectrum of HOD at the CCl_4/water interface. At mole fractions of 0.198 and 0.012 for HOD and H_2O, respectively, the SF signal in the OH stretching region originates primarily from HOD molecules.
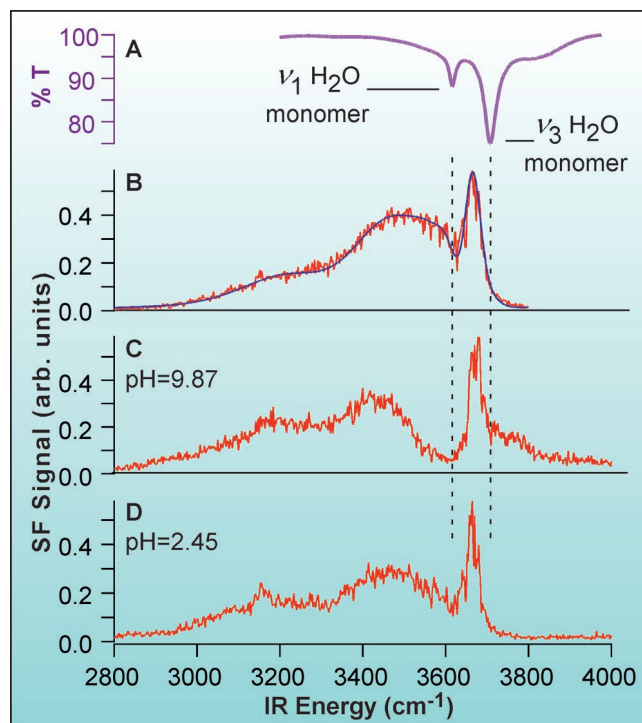

Fig. 3. Comparison of the vibrational spectrum of monomeric water in bulk CCl_4 to the VSF spectrum of the neat CCl_4/water interface for the aqueous phase at different pH values. (**A**) FTIR spectrum of CCl_4 with trace amounts of H_2O. The vertical axis is in percent transmittance (% T). (**B**) VSF spectrum of the neat CCl_4/H_2O interface at neutral pH, with the least-squares spectral fit to data superimposed as a blue solid line. The individual peaks composing the fit are shown in Fig. 4B. (**C**) VSF spectrum of the neat CCl_4/H_2O interface, with the aqueous-phase pH at 9.87. (**D**) VSF spectrum of the neat CCl_4/H_2O interface, with the aqueous-phase pH at 2.45. HCl and NaOH solutions were used to adjust the pH of the aqueous phase.

ments described above results in an excellent fit to the experimental data (Fig. 3B). The contributing spectral peaks and their respective phases derived from the best fit are shown in Fig. 4B along with a corresponding picture of these different interfacial water species and their orientation derived from the phase (Fig. 4A). The fit gives rise to SS and AS bands (no. 3 in Fig. 4) at 3618 ± 2 cm^{-1} and 3708 ± 2 cm^{-1} that coincide well with the SS and AS modes of water monomers in CCl$_4$. The frequencies and the phase (amplitude sign) of the peaks provide convincing evidence that whereas these water molecules have weak or negligible interactions with other water molecules, their interaction with the polarizable interfacial organic phase causes a net orientation of these molecules with their hydrogens pointed into the CCl$_4$, as depicted in Fig. 4B. The frequencies derived from the fit for the free OH and bonded OH modes (nos. 4 and 2) of water molecules that straddle the interface (Fig. 4B) also show good agreement with the HOD studies. The broad peak near 3250 cm^{-1} (no. 1) is attributed to the assembly of more strongly hydrogen-bonded interfacial water molecules that interact with interfacial and bulk-phase water molecules. Recent molecular dynamics simulations (30) of this interface are consistent with our observations.

The combined areas under the peaks corresponding to these oriented and weakly bonded water molecules [that is, those that straddle the interface (nos. 4 and 2) and in-terfacial water monomers/HB acceptors (no. 3)] make the most substantial contribution to the VSF spectrum and consequently represent the majority of the water molecules in the interfacial region. Although quantitative comparison of peak areas is complicated by the fact that increased hydrogen bonding results in stronger OH stretch intensity (17), such trends would support an even stronger dominance in the proportion of weakly interacting interfacial water molecules at these organic/water interfaces. The spectra do not provide support for commonly accepted models of an increase in the coordination number of water molecules at an organic/water interface and/or a strengthening of the hydrogen-bonding network between water molecules, both which would appear as a growth in intensity at lower frequencies rather than as an observed reduction in intensity in this region.
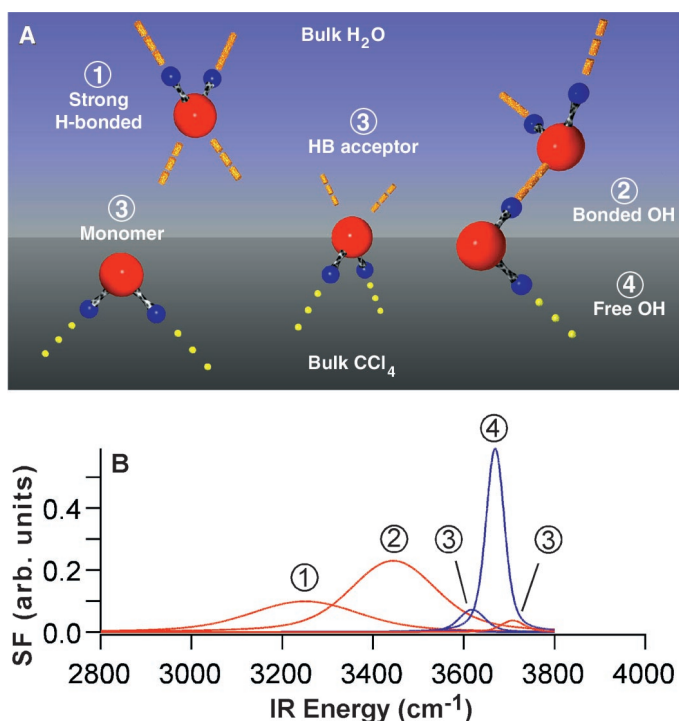
These studies demonstrate that dipolar interactions between interfacial water molecules and the polarizable organic phase play an important role in the interfacial region, resulting in strong orientation effects. The orientation of these water molecules that interact with the organic phase can be altered by changes in the pH of the aqueous phase. Such results have important implications for developing a molecular-level picture of some of the most important technological and biological processes in our everyday lives, including the penetration of water into lipids and macromolecular assemblies, chemical separations, interfacial polymerization, molecular transport, and macromolecular folding and assembly.

References and Notes
1. G. Hummer, S. Garde, A. E. García, M. E. Paulaitis, L. R. Pratt, *J. Phys. Chem. B* **102**, 10469 (1998).
2. S. H. Lee, P. J. Rossky, *J. Chem. Phys.* **100**, 3334 (1994).
3. K. Lum, D. Chandler, J. D. Weeks, *J. Phys. Chem. B* **103**, 4570 (1999).
4. S. Garde, G. Hummer, A. E. García, L. R. Pratt, *Phys. Rev. Lett.* **77**, 4966 (1996).
5. A. Wallqvist, B. J. Berne, *J. Phys. Chem.* **99**, 2893 (1995).
6. P. Linse, *J. Chem. Phys.* **86**, 4177 (1987).
7. I. Benjamin, *J. Chem. Phys.* **97**, 1432 (1992).
8. D. E. Gragson, G. L. Richmond, *J. Am. Chem. Soc.* **120**, 366 (1998).
9. Q. Du, R. Superfine, E. Freysz, Y. R. Shen, *Phys. Rev. Lett.* **70**, 2313 (1993).
10. A nanosecond Nd:yttrium-aluminum-garnet pumped, double-pass, optical parametric oscillator/amplifier was used to deliver 1 to 2 mJ of mid-IR and 4 mJ of 532-nm pulses to the interface for both the CCl$_4$/H$_2$O and the alkane/water systems. The air/water spectrum was taken with a 2-ps laser system overlapping 275 μJ of 800-nm and 3 to 5 μJ of mid-IR radiation on the interface in an external reflection geometry. As the tunable IR beam scans over the frequency of a vibrational mode of the interfacial molecule, the SF process is resonantly enhanced and a vibrational spectrum of interfacial molecules results.
11. G. A. Jeffrey, *An Introduction to Hydrogen Bonding* (Oxford Univ. Press, New York, 1997).
12. VSF spectra of the CCl$_4$/water interface [CCl$_4$: Aldrich, 99.9% high-performance liquid chromatography (HPLC) grade, doubly distilled; H$_2$O: Mallinckrodt ChromAR HPLC Grade H$_2$O] were collected so that both IR and visible beams passed through an IR-grade quartz prism and a ~2-mm path length of CCl$_4$, where they were totally internally reflected off of the CCl$_4$/H$_2$O interface. This experimental design permits the use of small solvent volumes, which combined with extensive solvent purification procedures eliminates trace impurities that naturally concentrate at this interface. VSF spectra of the hexane/water (hexane: Aldrich, 99+%, doubly distilled) interface were collected using a ~1-mm layer of hexane placed between water and an IR-grade quartz prism, allowing examination of the hexane/water interface under a total internal reflection geometry. VSF experiments at the air/water (Mallinckrodt ChromAR HPLC Grade H$_2$O) interface were performed in a N$_2$ purged closed cell so that contamination of the interface was eliminated (beyond detectable levels). Our most detailed studies are with CCl$_4$, where spectral absorption of the incident IR beam is minimized.
13. D. Eisenberg, W. Kauzmann, *The Structure and Properties of Water* (Oxford Univ. Press, New York, 1969).
14. Q. Du, E. Freysz, Y. R. Shen, *Science* **264**, 826 (1994).
15. D. F. Coker, R. E. Miller, R. O. Watts, *J. Chem. Phys.* **82**, 3554 (1985).
16. M. P. Conrad, H. L. Strauss, *J. Phys. Chem.* **91**, 1668 (1987).
17. J. R. Scherer, in *Advances in Infrared and Raman Spectroscopy*, R. J. H. Clark, R. E. Hester, Eds. (Heyden, Philadelphia, 1978), vol. 5, pp. 149–216.
18. All of the organic/water interfaces studied have been found to be highly sensitive to trace impurities that tend to concentrate at the interface and can cause the spectrum to appear more like that of the air/water system (Fig. 1C). This effect can readily account for the differences between our observations and previous CCl$_4$/H$_2$O (21) and hexane/H$_2$O (14) VSF studies.
19. The calculated binding energy for the H$_2$O-CCl$_4$ dimer is reported to be -1.4 kcal/mol (30).
20. FTIR isotopic exchange studies in bulk CCl$_4$ were performed in a 1-cm path length IR-grade quartz cell at 295 K. D$_2$O (Cambridge Isotope Laboratories, 99.996%) was shaken over doubly distilled

Fig. 4. Water molecules present at the neat CCl$_4$/H$_2$O interface. (**A**) Schematic of the water molecules in the VSF spectrum of the neat CCl$_4$/H$_2$O interface, corresponding to the peaks in the spectrum of (**B**). Dashed lines represent H$_2$O-H$_2$O interactions, and dotted lines represent H$_2$O-CCl$_4$ interactions. (**B**) Peak positions for the various OH modes derived from the fit to the data in Fig. 3B. Each fitted peak is shaded either blue (+) or red (−), identifying the relative phase of the molecular vibration. Peak parameters [peak position, full width at half maximum, and peak intensity (followed by amplitude sign in parentheses)] are as follows: 3250 cm^{-1}, 284 cm^{-1}, 0.32 (−); 3444 cm^{-1}, 220 cm^{-1}, 0.50 (−); 3575 cm^{-1}, 70 cm^{-1}, 0.08 (+); 3618 cm^{-1}, 66 cm^{-1}, 0.30 (+); 3669 cm^{-1}, 44 cm^{-1}, 0.88 (+); and 3707 cm^{-1}, 60 cm^{-1}, 0.21 (−).

CCl$_4$ (Aldrich, 99.9% HPLC grade), which produces HOD by isotopic exchange with trace amounts of H$_2$O.
21. D. E. Gragson, G. L. Richmond, *J. Phys. Chem. B* **102**, 569 (1998).
22. J. L. Green, A. R. Lacey, M. G. Sceats, *Chem. Phys. Lett.* **130**, 67 (1986).
23. J. P. Devlin, *J. Chem. Phys.* **90**, 1322 (1989).
24. E. Zoidis, J. Yarwood, T. Tassaing, Y. Danten, M. Besnard, *J. Mol. Liq.* **64**, 197 (1995).
25. T. T. Wall, D. F. Hornig, *J. Chem. Phys.* **43**, 2079 (1965).
26. The phase of a particular molecular vibration is reflected by the positive/negative sign associated with the amplitude parameter derived from the fitted data.
27. M. G. Brown, E. A. Raymond, H. C. Allen, L. F. Scatena, G. L. Richmond, *J. Phys. Chem* **104**, 10220 (2000).
28. J. Lobau, K. Wolfrum, *J. Opt. Soc. Am. B* **14**, 2505 (1997).
29. C. Hirose, N. Akamatsu, K. Domen, *Appl. Spectrosc.* **46**, 1051 (1992).
30. T. Chang, L. X. Dang, *J. Chem. Phys.* **104**, 6772 (1996).
31. The authors gratefully acknowledge NSF (grant CHE-9725751) for support of the liquid/liquid studies; the U.S. Department of Energy, Basic Energy Sciences, for the air/water studies; and the Office of Naval Research for equipment funding.

Controlled Rotation of Optically Trapped Microscopic Particles

L. Paterson,[1] M. P. MacDonald,[1] J. Arlt,[1] W. Sibbett,[1] P. E. Bryant,[2] K. Dholakia[1]*

We demonstrate controlled rotation of optically trapped objects in a spiral interference pattern. This pattern is generated by interfering an annular shaped laser beam with a reference beam. Objects are trapped in the spiral arms of the pattern. Changing the optical path length causes this pattern, and thus the trapped objects, to rotate. Structures of silica microspheres, microscopic glass rods, and chromosomes are set into rotation at rates in excess of 5 hertz. This technique does not depend on intrinsic properties of the trapped particle and thus offers important applications in optical and biological micromachines.

Optical forces have been used to trap and manipulate micrometer-sized particles for more than a decade (*1*). Since it was shown that a single tightly focused laser beam could be used to hold, in three dimensions, a microscopic particle near the focus of the beam, this optical tweezers technique has now become an established tool in biology, enabling a whole host of studies. They can be used to manipulate and study whole cells such as bacterial, fungal, plant, and animal cells (*2*) or intracellular structures such as chromosomes (*3*). Optical tweezers make use of the optical gradient force. For particles of higher refractive index than their surrounding medium, the laser beam induces a force attracting the trapped particle into the region of highest light intensity.

The ability to rotate objects offers a new degree of control for microobjects and has important applications in optical micromachines and biotechnology. Various schemes have, therefore, been investigated recently to induce rotation of trapped particles within optical tweezers. This could be used to realize biological machines that could function within living cells or optically driven cogs to drive micromachines.

Besides the use of specially fabricated microobjects (*4*), two major schemes have successfully enabled trapped microobjects to be set into rotation. The first scheme uses Laguerre-Gaussian (LG) light beams (*5–7*). These beams have an on-axis phase singularity and are characterized by helical phase fronts (Fig. 1A). The Poynting vector in such beams follows a corkscrewlike path as the beam propagates, and this gives rise to an orbital angular momentum component in the light beam (*8*). This angular momentum is distinct from any angular momentum due to the polarization state of the light and has a magnitude of $l\hbar$ per photon. Specifically, l refers to the number of complete cycles of phase ($2\pi l$) upon going around the beam circumference. However, to transfer orbital angular momentum to a trapped particle with such a beam, the particle must typically absorb some of the laser light yet still be transparent enough to enable tweezing to occur. This in turn restricts the range of particles to which this method can be applied, and it also further limits this technique because any heating that arises from this absorption could damage the rotating particle. Furthermore, as the particle absorption can be difficult to quantify, controlled rotation of trapped objects in such a beam is very difficult to realize.

The other technique for rotation makes use of the change in polarization state of light upon passage through a birefringent particle (*9*, *10*). For example, circularly polarized light has spin angular momentum

that can be exchanged with a birefringent medium (e.g., calcite) upon propagation of the beam through the medium. This is analogous to Beth's famous experiment—where he measured the torque on a suspended half-wave plate as circularly polarized light passed through it (*11*)—but here we are working on a microscopic scale. This method has shown rotation rates of a few hundred hertz for irregular samples of crushed calcite, but it is difficult to control and is limited solely to birefringent media so it is not widely applicable. Although both of these methods have proven useful in specific applications, they do have serious shortcomings for general applications in rotating optical microcomponents and realizing optical micromachines.

We introduce a general scheme for rotating trapped microobjects. Specifically, we trap objects within the interference pattern of an LG beam and a plane wave (Fig. 1B) (*12*). By changing the path length of the interferometer, we are able to cause the spiral
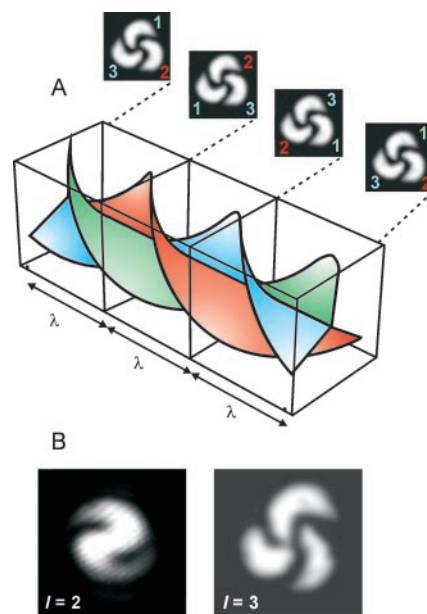

Fig. 1. (A) The phase fronts of an LG beam of azimuthal index $l = 3$ (helical structure) and intensity pattern when interfered with a plane wave. The phase fronts describe a triple start intertwined helix that repeats its shape every λ but only rotates fully after $l\lambda$. In (**B**), we can see the experimental forms of the interference patterns of LG beams of index $l = 2$ and $l = 3$ with plane waves used in our experiments.

[1]School of Physics and Astronomy, St. Andrews University, North Haugh, St. Andrews, Fife KY16 9SS, Scotland. [2]School of Biology, Bute Building, St. Andrews University, St. Andrews, Fife KY16 9TS, Scotland.

*To whom correspondence should be addressed. E-mail: kd1@st-and.ac.uk